# Phase multistability and phase synchronization in an array of locally coupled period-doubling oscillators

A. Shabunin,[1,2] U. Feudel,[2] and V. Astakhov[1]
[1]*Physical Faculty, Saratov State University, Astrakhanskaya Str., Saratov 410012, Russia*
[2]*Theoretical Physics/Complex Systems, ICBM, Carl von Ossietzky Universität Oldenburg, PF 2503, D-26111 Oldenburg, Germany*
(Received 20 March 2009; published 20 August 2009)

We consider phase multistability and phase synchronization phenomena in a chain of period-doubling oscillators. The synchronization in arrays of diffusively coupled self-sustained oscillators manifests itself as rotating wave regimes, which are characterized by equal amplitudes and phases in every site which are shifted by a constant value. The value of the phase shift is preserved while the shape of motion becomes more complex through a period-doubling cascade. The number of coexisting attractors increases drastically after the transition from period-one to period-two oscillations and then after every following period-doubling bifurcation. In the chaotic region, we observe a number of phase-synchronized modes with instantaneous phases locked in different values. The loss of phase synchronization with decreasing coupling is accompanied by intermittency between several synchronous regimes.

DOI: 10.1103/PhysRevE.80.026211 PACS number(s): 05.45.Xt

## I. INTRODUCTION

Synchronization of oscillations in coupled systems is one of the fundamental properties of nature, which has many applications in different fields of science and technology: arrays of coupled lasers [1] and Josephson junctions [2], networks of electronics oscillators [3], reaction-diffusion systems [4], etc. If oscillators are periodic, their synchronization manifests in two interconnected phenomena: (a) adjustment of their periods and (b) locking of the instantaneous phases. In the last case, the difference between the phases of neighboring oscillators $\Delta\varphi(t)$, being arbitrary in the asynchronous state, takes some determined stationary value $[\Delta\varphi(t)=\Delta\varphi^{(1)}]$ after synchronization. Some systems allow several values of stationary phase shifts $\{\Delta\varphi^{(1)},\Delta\varphi^{(2)},\ldots,\Delta\varphi^{(M)}\}$, where everyone corresponds to its own attractor. In this case, the system demonstrates "phase multistability" (PM) [5]. Hence, phase multistability is a special type of multistability observed in coupled systems, when coexisting attractors have equal (or very close) dynamical characteristics (amplitudes, frequencies, etc.), but differ by the phase shifts between time series in the subsystems. If the shape of oscillations is simple (close to harmonic oscillations), a system of two coupled oscillators typically demonstrates only one synchronous state (however, there are exceptions, see, for example, [6]). When the form of oscillations becomes more complex (for example, as a result of period-doubling bifurcations), the number of coexisting phase modes may increase. This scenario was described in detail in a number of works [5,7]. In particular, in systems of two symmetrically coupled identical period-doubling oscillators, the number of coexisting attractors doubles after every period-doubling bifurcation if the coupling is sufficiently small. As a result, at the threshold to chaos the system demonstrates an infinite number of coexisting stable states. In the chaotic region, the number of attractors begins to decrease as a consequence of band-merging bifurcations, which are accompanied by merging of the attractors. This process ends with the appearance of a single one-band chaotic attractor. In [8], it was shown that the formation of multistability takes place through the same bifurcation mechanism as the process of loss of complete synchronization of chaos. Transverse period-doubling bifurcations of the main family of saddle periodic orbits play the key role in both phenomena.

In ensembles of more than two oscillators, the coexisting synchronous regimes characterized by different phase shifts are observed already on the stage of simple oscillations. For large chains, they can be considered as waves running along the discrete medium with a constant phase speed [running waves and rotating waves (RWs)] [9]. This type of spatial organization is of great importance for certain engineering applications such as in the design of antenna systems. It also can take place in behavior of some biological systems [10]. Bifurcation analysis of different phase modes in ensembles of harmonic oscillators for different types of coupling has been studied in [11]. In [12], it was demonstrated that bistability of elements of the chain can lead to the appearance of stationary spatial disorder. The possibility of the appearance of new effects due to the complication of the form of oscillations was investigated in [13].

A large body of research has been devoted to simple periodic oscillators or just to phase equation models. However, RW can exist also for arrays of elements with complex chaotic behavior. Chaotic rotating waves (CRWs) have been observed in a number of works [14]. The transition from periodic to chaotic RW in a ring of diffusively coupled self-sustained oscillators with period-doubling bifurcations was described in [15]. It was shown that on the plane of parameters, "coupling-excitation" RW with different spatial periods forms an encapsulated structure. Regions of regimes with shorter wavelengths are contained inside regions with longer wavelengths. While increasing the parameter of excitation on the base of each periodic RW, a set of period-doubling bifurcations takes place leading to a complication of oscillations as well as bifurcations where tori are born. As a result of this evolution, chaotic RWs appear, which are characterized by the same spatial periodicity as the original periodic RW. With further development of chaos, different CRWs unite into a spatially and temporally chaotic mode. The described scenario gives a general picture of the complication of spa-

 

tiotemporal dynamics in arrays of coupled period-doubling oscillators. However, some questions remain unanswered: (a) how is the spatial order observed for RW connected with the synchronization between oscillators? (b) How many different attractors coexist in phase space and how does their number change with period-doubling bifurcations? (c) Is it possible to find some common classification for different coexisting attractors? (d) Are these regimes typical or is it only possible to find them with a specific choice of the initial values? (e) Can other than RW oscillatory regimes be found in phase space? An attempt to find answers to these questions, as well as to give a general and sufficiently detailed description of processes of multistability formation and synchronization in arrays of coupled period-doubling oscillators, is the main stimulus to this research.

The paper is organized as follows. Section II outlines common properties of the oscillations under study and carries out a simple analysis of their stability with respect to perturbations in the harmonic approximation. It does not contain principally new results but gives some necessary definitions introducing the subject of research. In Sec. III we consider period-one RW regimes in a ring of Rössler oscillators and evaluate how typical they are from the point of view of initial values. Section IV describes the evolution of the waves with parameter changes from periodic to chaotic oscillations. Section V is devoted to common regularities of the formation of multistability in the system. There we make an attempt to calculate coexisting attractors and give their common classification in terms of their phase spectrum. Section VI is devoted to chaotic RW considering them from the point of view of phase synchronization. The last section summarizes the results.

## II. OSCILLATING REGIMES UNDER STUDY AND THE ANALYSIS OF STABILITY OF SIMPLE OSCILLATIONS

Let us consider a finite array of coupled identical oscillators with symmetric diffusive coupling,

$$\dot{\mathbf{x}}_i = \mathbf{f}(\mathbf{x}_i, \varepsilon) + \hat{\gamma}(\mathbf{x}_{i+1} - \mathbf{x}_i) + \hat{\gamma}(\mathbf{x}_{i-1} - \mathbf{x}_i), \tag{1}$$

where $\mathbf{x}_i$ is the $L$-dimensional vector of dynamical variables of the $i$th oscillator $(i=1,2,3,\ldots,N)$, $\mathbf{f}$ is the vector function defining its internal dynamics, $\varepsilon$ is the control parameter, while $\hat{\gamma}$ is the positively defined coupling matrix. Here and further, we will use periodic boundary conditions $\mathbf{x}_0=\mathbf{x}_N$, $\mathbf{x}_{N+1}=\mathbf{x}_1$. We suppose that without coupling each oscillator exhibits limit-cycle oscillations, the shape of which is close to harmonic oscillations $\mathbf{x}_i(t)=\boldsymbol{\xi}_i(t)$. Here $\boldsymbol{\xi}_i(t+T)=\boldsymbol{\xi}_i(t)$ are $T$-periodic functions of time, whose shape is close to a cosine function. Since all oscillations are identical and autonomous, all functions $\boldsymbol{\xi}_i$ are the same up to some arbitrary time shifts $(\tau_i)$: $\boldsymbol{\xi}_i(t)=\boldsymbol{\xi}(t+\tau_i)$. The particular values of $\tau_i$ are defined by the initial condition.

From the projection of the trajectory of system (1) to the subspace of each oscillator $x_i$, we can define the instantaneous phase $\varphi_i(t)$ of oscillations in the site $i$, which characterizes the current location of the phase point on the limit cycle. Here we define the phase as a piecewise linear, $T$-periodic function of time, taking values within the interval $[-\pi;\pi]$,

$$\varphi_i(t) = 2\pi\frac{t-t_n}{t_{n+1}-t_n} - \pi, \tag{2}$$

where $t_n$ $(n=1,2,3,\ldots)$ are points of subsequent unidirectional intersections of the trajectory $\mathbf{x}_i(t)$ with some transverse $(NL-1)$-dimensional manifold. Differences between phases in neighboring oscillators

$$\Delta\varphi_i(t) = \varphi_{i+1}(t) - \varphi_i(t), \quad (i=1,2,\ldots,N) \tag{3}$$

will be called phase shifts between the oscillations. Since all oscillators have equal periods, the phase shifts do not change with time taking constant values $\Delta\varphi_i(t)=\mathcal{C}_i$. Due to periodic boundary conditions, the whole sum of them along the array $\Phi=\Sigma_{i=1}^{N}\mathcal{C}_i$ must be proportional to $2\pi$: $\Phi=2\pi k$, where the index $k\in[-N/2:N/2]$ is an integer value.

Coupling between the oscillators synchronizes them. The synchronization removes the uncertainty of differences in the instantaneous phases. They take determined values, which do not depend anymore continuously on the initial condition, but are defined by the properties of the system. Chains of identical oscillators [Eq. (1)] permit states with phase-shift constants, which are equal to each other: $\Delta\varphi_i(t)=\Delta\varphi$. In this case, oscillations in every point of the discrete medium have equal amplitudes, periods, and other dynamical characteristics but differ from each other by the constant phase shift. Such oscillations can be considered as waves, rotating with a phase velocity $v=2\pi/(T\Delta\varphi)$ along the ring, with the corresponding wavelength $\Lambda=2\pi/\Delta\varphi$. For the chain of finite length $N$, the number of possible RW $M$ is finite and equal to $N$, while the particular value of $\Delta\varphi$ can be found from the index $k$,

$$\Delta\varphi^{(k)} = \frac{2\pi k}{N}. \tag{4}$$

So, depending on $k$, every RW has its value of $v=N/Tk$ and $\Lambda=N/k$. Further, we will use $k$ as an index, which classifies a rotating wave, since its value determines its spatial characteristics. Simple periodic RW will be denoted as $1C^k$, where the first numerical index $(1,2,4,8,\ldots)$ denotes the periodicity of the limit cycle, the letter $C$ points out the periodic temporal behavior (cycle), while the upper index defines the spatial structure of the wave. The waves of higher temporal periods will be noted as $2C^k$, $4C^k$, etc.

The value $k=0$ relates to the spatially homogeneous regime of in-phase oscillations, $k=\pm N/2$ relates to antiphase oscillations in neighboring sites. Other positive values of $k$ define RW rotating in the positive direction (forward wave), while the corresponding negative values $-k$ define the same RW but rotating in the negative direction (backward wave). Both forward and backward waves have the same characteristics except for their directions, hence, we focus only on forward waves. If $\Lambda=N/k$ is an integer value, oscillations in the $i$th and the $(i+\Lambda)$th sites are in phase. This oscillation is spatially periodic with spatial period $\Lambda$.

The RW described above corresponds to possible oscillating modes of the ring. To analyze their stability let us consider system (1) near the point of Andronov–Hopf bifurcation on the example of coupled Van der Pol generators,

$$\mathbf{f}(\mathbf{x}) = \begin{bmatrix} y \\ (\varepsilon - x^2)y - x \end{bmatrix},$$

with scalar coupling

$$\hat{\gamma} = \begin{bmatrix} \gamma & 0 \\ 0 & 0 \end{bmatrix}.$$

With these assumptions, the behavior of the ring can be described by the equations for the complex scalar amplitudes $a_i$,

$$\dot{a}_i = \frac{\varepsilon}{2}a_i - \frac{|a_i|^2 a_i}{8} + \frac{\gamma}{2}(a_{i+1} + a_{i-1} - 2a_i), \quad i = 1,2,\ldots,N, \tag{5}$$

where $\varepsilon \geq 0$ governs the amplitude of the periodic oscillations in the uncoupled element. It grows as $\sqrt{\varepsilon}$. Writing Eq. (5) in polar coordinates $\rho_i \geq 0$ and $-\pi \leq \varphi_i \leq \pi$, we get equations for the real amplitudes and phases,

$$\dot{\rho}_i = \frac{\varepsilon}{2}\rho_i - \frac{\rho_i^3}{8} + \frac{\gamma}{2}[\rho_{i+1}\cos(\varphi_{i+1} - \varphi_i) + \rho_{i-1}\cos(\varphi_{i-1} - \varphi_i) - 2\rho_i], \tag{6}$$

$$\dot{\varphi}_i = \frac{\gamma}{2}\left[\frac{\rho_{i+1}}{\rho_i}\sin(\varphi_{i+1} - \varphi_i) + \frac{\rho_{i-1}}{\rho_i}\sin(\varphi_{i-1} - \varphi_i)\right]. \tag{7}$$

Equilibrium points of Eqs. (6) and (7) correspond to limiting periodic oscillations with $T=1$ in the original system: $x_i(t) = \rho_i \cos(t+\varphi_i)$. If all the amplitudes and phase shifts are equal to each other $(\rho_i = \rho, \varphi_{i+1} - \varphi_i = \varphi_i - \varphi_{i-1} = \Delta\varphi^{(k)} = \frac{2\pi k}{N})$, we obtain equations, which describe the rotating wave with a given $k$,

$$\rho^{(k)} = \frac{\acute{\varepsilon}_k}{2}\rho^{(k)} - \frac{(\rho^{(k)})^3}{8}, \tag{8}$$

$$\varphi^{(k)} = 0, \tag{9}$$

where

$$\acute{\varepsilon}_k = \varepsilon - 2\gamma[1 - \cos(\Delta\varphi^{(k)})]. \tag{10}$$

The form of Eqs. (8) and (9) coincides with the equation for the single-uncoupled oscillator if the excitation parameter is recalculated according to Eq. (10). Hence, similarly to the uncoupled oscillator, the trivial solution $\rho=0$ bifurcates on lines $\varepsilon = 2\gamma[1-\cos(\Delta\varphi_k)]$ with the birth of a new periodic solution with amplitude $\rho^{(k)} = 2\sqrt{\acute{\varepsilon}_k}$. With changing $k$, there is a sequence of equal bifurcations. If $\gamma \geq 0$, the first bifurcation takes place on the line $\varepsilon = 0$. This leads to the appearance of stable spatially homogeneous oscillations $(1C^0)$. After the bifurcation, the trivial solution becomes a saddle. Then, on each line $\varepsilon = 2\gamma[1-\cos(2k\pi/N)]$ $(k=1,2,\ldots,N/2-1)$ one more eigenvalue crosses the imaginary axis. In this bifurcation, two waves are born: $1C^k$ and $1C^{-k}$ running in opposite directions. So, with increasing $\varepsilon$ we observe a sequence of bifurcations which give birth to RW of shorter and shorter wavelengths. The last bifurcation occurs for $k=N/2$ on the line $\varepsilon = 4\gamma$. If $\gamma < 0$, the scenario is the opposite. The stable solution $\rho=0$ bifurcates on the line $\varepsilon = 4\gamma$ with the appearance of stable antiphase oscillations $1C^{N/2}$. In the following bifurcations, saddle waves of longer and longer wavelengths are born until the appearance of spatially homogeneous oscillations on the line $\varepsilon=0$. Further, we will consider only positive coupling values.

All RW regimes, except the spatially homogeneous one, are unstable in the moment of their emergence. To find regions of their stability, we use the standard technique of linear stability analysis in the neighborhood of the chosen solutions (8) and (9). For arrays of diffusively coupled oscillators, this method was described in [16,17]. The matrix of linearization of Eqs. (6) and (7) has the following form:

$$[J] = \begin{bmatrix} [A_0] & [A_1] & 0 & 0 & \ldots & [A_{-1}] \\ [A_{-1}] & [A_0] & [A_1] & 0 & \ldots & 0 \\ 0 & [A_{-1}] & [A_0] & [A_1] & \ldots & 0 \\ & & & & \ldots & \\ [A_1] & 0 & 0 & 0 & \ldots & [A_0] \end{bmatrix}, \tag{11}$$

where $[A_{-1}]$, $[A_0]$, and $[A_1]$ are the $2\times 2$ matrices,

$$[A_{-1}] = \begin{bmatrix} \frac{\gamma}{2}\cos(\Delta\varphi^{(k)}) & \frac{\gamma\rho^{(k)}}{2}\sin(\Delta\varphi^{(k)}) \\ -\frac{\gamma}{2\rho^{(k)}}\sin(\Delta\varphi^{(k)}) & \frac{\gamma}{2}\cos(\Delta\varphi^{(k)}) \end{bmatrix},$$

$$[A_0] = \begin{bmatrix} -\acute{\varepsilon}_k - \gamma\cos(\Delta\varphi^{(k)}) & 0 \\ 0 & -\gamma\cos(\Delta\varphi^{(k)}) \end{bmatrix},$$

$$[A_1] = \begin{bmatrix} \frac{\gamma}{2}\cos(\Delta\varphi^{(k)}) & -\frac{\gamma\rho^{(k)}}{2}\sin(\Delta\varphi^{(k)}) \\ \frac{\gamma}{2\rho^{(k)}}\sin(\Delta\varphi^{(k)}) & \frac{\gamma}{2}\cos(\Delta\varphi^{(k)}) \end{bmatrix}.$$

Since matrix (11) is right circular, its eigenvalues can be easily found,

$$\lambda_{0,1}^{(k)} = 0, \tag{12}$$

$$\lambda_{0,2}^{(k)} = -\acute{\varepsilon}_k, \tag{13}$$

$$\lambda_{i,1}^{(k)} = -\frac{\acute{\varepsilon}_k}{2} + \sqrt{\frac{\acute{\varepsilon}_k^2}{4} + \gamma^2\sin^2(\Delta\varphi^{(k)})\sin^2(2\pi i/N)} - \gamma\cos(\Delta\varphi^{(k)})[1-\cos(2\pi i/N)], \tag{14}$$

$$\lambda_{i,2}^{(k)} = -\frac{\acute{\varepsilon}_k}{2} - \sqrt{\frac{\acute{\varepsilon}_k^2}{4} + \gamma^2\sin^2(\Delta\varphi^{(k)})\sin^2(2\pi i/N)} - \gamma\cos(\Delta\varphi^{(k)})[1-\cos(2\pi i/N)], \tag{15}$$

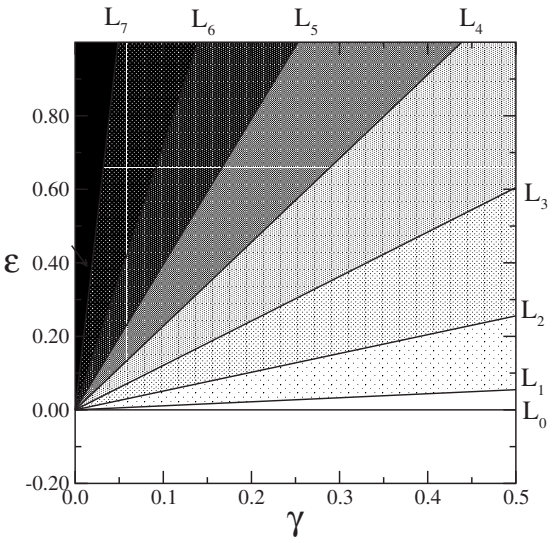


FIG. 1. Regions of stability of harmonic RW for the chain (5) with 30 oscillators. The regions themselves are marked by different grayscales from white for $1C^0$ to black for $1C^7$. The darker color relates to the shorter wave. Lines $L_k$ denote the boundaries of the regions for the correspondent waves $C^k$.

$$i = 1, \ldots, N-1.$$

The zero eigenvalue $\lambda_{0,1}$ reflects the invariance of the solution to the choice of the initial phase. The bifurcation condition for the eigenvalue $\lambda_{0,2}$: $\acute{\varepsilon}_k=0$, relates to the bifurcations of $\rho=0$ described above. Hence, the inequality $\acute{\varepsilon}_k \geq 0$ defines the region of existence of the considered regime $(\rho_i^{(k)}; \varphi_i^{(k)})$, while its stability is determined by Eqs. (14) and (15). The latter ones give us the region of stability in the plane $\gamma-\varepsilon$, which is determined by the following inequalities:

$$\varepsilon \geq \gamma\left[2 - 4\cos(\Delta\varphi_k) + \frac{1+\cos(2\pi/N)}{\cos(\Delta\varphi_k)}\right], \tag{16}$$

$$\gamma\cos(\Delta\varphi_k) > 0. \tag{17}$$

Let us analyze the formulas (16) and (17). From Eq. (17), it is seen that $\Delta\varphi^{(k)}$ must be less than $\pi/2$; therefore, only a part of $N$ rotating wave regimes can be found as stable for $\gamma>0$. For a chain of $N$ oscillators, the number of coexisting modes $M$ must be the integer part of the value $N/4$, if $N$ is not proportional to 4. In the limiting case, when $N=4n$, $n=1,2,3,\ldots$ some of the waves (with $\Delta\varphi^{(k)}=\pi/2$) are neutrally stable. The latter is not observed at nonzero positive coupling. However, the $\pi/2$ waves with more complex oscillations can exist at positive coupling. Therefore, the case of $N=4n$ appears to be more complex for the analysis of multistability and needs a special consideration.

Figure 1 depicts regions of stability for the chain [Eqs. (8) and (9)] of $N=30$ oscillators. For this length, $k$ can take values $0,1,\ldots,15$; however, only some of them $(0\leq k\leq 7)$ can be found to be stable since only for them $\Delta\varphi^{(k)}<\pi/2$. Thus, the line $\gamma=0$ divides the parameter plane into regions with long-wavelength regimes $1C^0 \ldots 1C^7$ $(\gamma>0)$ and short-wavelength ones $1C^8 \ldots 1C^{15}$ $(\gamma<0)$. The regions of stability of RW are denoted by $L_k$. They are defined by the equation,

$$\varepsilon = \gamma\left[2 - 4\cos(\Delta\varphi_k) + \frac{1+\cos(2\pi/N)}{\cos(\Delta\varphi_k)}\right].$$

The regions themselves are marked by different gray scales from white for $1C^0$ to black for $1C^7$. The darker color relates to the shorter wave. Here, we see an embedded structure of multistability. At small coupling, there exists any rotating wave with $\Delta\varphi_k<\pi/2$. Increasing $\gamma$ leads to the elimination of shorter waves, while the longer ones still exist. At last, when the coupling is strong enough only spatially homogeneous oscillations survive in the system. Showing the stability diagram for harmonic oscillations, Fig. 1 gives us a first approximation of the structure in the parameter plane for real unharmonic oscillators. At least we can expect a similar structure for period-one oscillations, though the structure for more complex periodic or chaotic oscillations remains an open question.

## III. SYSTEM UNDER STUDY AND THE SIMPLE RW

Now, let us come to the analysis of arrays of oscillators with more complex behavior, which demonstrate a transition from simple period-one to high-period periodic and chaotic oscillations via a cascade of period-doubling bifurcations. For numerical simulations, we choose a ring of coupled Rössler oscillators, which represents one of the basic models of nonlinear dynamics [18]. The equations of the system are

$$\begin{aligned}
\dot{x}_i &= -y_i - z_i + \gamma(x_{i+1} - 2x_i + x_{i-1}),\\
\dot{y}_i &= x_i + 0.2y_i,\\
\dot{z}_i &= 0.2 + z_i(x_i - c).
\end{aligned} \tag{18}$$

Here $x_i$, $y_i$, and $z_i$ are the dynamical variables of the $i$th oscillator $(i=1,\ldots,N)$, $c$ is a control parameter, which governs the dynamics of the uncoupled oscillator, while $\gamma>0$ is the parameter of a scalar diffusive coupling. The number of oscillators was chosen as $N=30$.

Systems (18) were investigated by means of numerical simulations from different initial values. The resulting time series in the long term limit was analyzed by phase portraits, Poincaré sections, power spectrum,

$$P_i(f) = \langle F_i(f)F_i^*(f)\rangle,$$

[where $F_i(f)$ is the Fourier transform of $x_i(t)$, while $f$ is the frequency] and phase cross spectrum between $x_i(t)$ and $x_{i+1}(t)$ oscillations

$$\Delta\theta_i(f) = \theta_{i+1}(f) - \theta_i(f)$$

[$\theta_i$ is the Fourier phase of $x_i$: $F_i(f)=|F_i(f)|\exp(j\theta_i(f))$]. All used spectral characteristics are based on well-defined methods of spectral analysis (see, for example, [19]). The Poincaré map is used for visualization of the spatial structure of RW. We search for the moments $t_n$ when the variable $y_1$ changes its sign from positive to negative, plotting the cor-

responding values of $x_i(t_n)$ versus $i$. The plots represent "snapshots" of the wave at time instants related to the fixed value of the phase in the first oscillator. This method has been described in [15].

To begin with, we consider simple rotating waves at small coupling $\gamma=0.005$. At $0.4<c<2.85$, oscillations in the chain are one periodic. Let us choose the parameter $c=2.35$. According to the preliminary analysis in Sec. II, we can expect RW with index $k=0,1,\ldots,7$. The choice of the particular RW regime is determined by the choice of the initial values. To get the RW with given $k$, we must choose the initial distribution of the variables sufficiently close to the desired wave. One of the possible ways to realize this is to set the initial values of $x_i$ and $y_i$ as sine and cosine functions with phases $i\Delta\phi$ and choose $\Delta\phi=\Delta\varphi^{(k)}$,

$$x_i = X_0 \sin(i\Delta\phi),$$

$$y_i = Y_0 \cos(i\Delta\phi),$$

$$z_i = 0,$$

$$i = 0,1,\ldots,N-1, \tag{19}$$

where $X_0$ and $Y_0$ are chosen sufficiently close to the amplitudes of $x$ and $y$ variables in the uncoupled oscillator. The numerical simulation shows that this procedure leads to the desired results. All expected RW can be found as stable. Figure 2 depicts the snapshots of the waves with $k=0$, 1, 2, 4, and 7 (the left-hand column) and the cross projections of phase portraits in the variables $x_1$-$x_2$ (the right-hand column) obtained at $c=2.35$. The structure of the snapshots is seen to be determined by the index $k$. Its value is equal to the number of minima and maxima along the chain. In the figure, we also show the snapshots of the backward waves by dotted lines.

All oscillations presented in Fig. 2 have equal amplitudes and periods in every site and phases that are equidistantly distributed along the array. Figure 3 plots the power spectrum of $x_1(t)$ and the phase cross spectrum of $x_1(t)$ and $x_2(t)$ oscillations for the $1C^2$ mode. The power spectrum contains the main harmonic at frequency $f_0\simeq 0.17$ and its higher harmonics at $2f_0$, $3f_0$, etc. The value of the phase of the main harmonic $\Delta\theta_1^{(1)}=\Delta\theta_1(f_0)$ is exactly equal to the value of the instantaneous phase shift for this mode $\Delta\theta_1^{(1)}=-4\pi/30\simeq -0.42$. The phases of higher harmonics are proportional to it: $\Delta\theta(nf_0)=n\Delta\theta^{(1)}$. The power and phase cross spectrum of other $x_i$ $(i=2,3,\ldots,N-1)$ oscillations are the same as of $x_1$.

So, we see that at small coupling and chosen $c$ the systems (18) are characterized by phase multistability. Do other than $1C^0-1C^7$ waves or regimes with nonuniform distribution of phases exist in phase space? Let us set the initial values according to Eqs. (19) but use arbitrary values of $\Delta\phi$. Choosing the initial values this way, we have carried out numerical simulations to study the dependence of the resulting regime type on the angle $\Delta\phi$. The results are depicted in Fig. 4. Choosing initial values according to Eqs. (19) with $0\leq\Delta\phi\leq\pi$, we have got all predicted RW regimes. None of the regimes, except $1C^0-1C^7$, has been observed at the described choice of the initial values. At small values of the

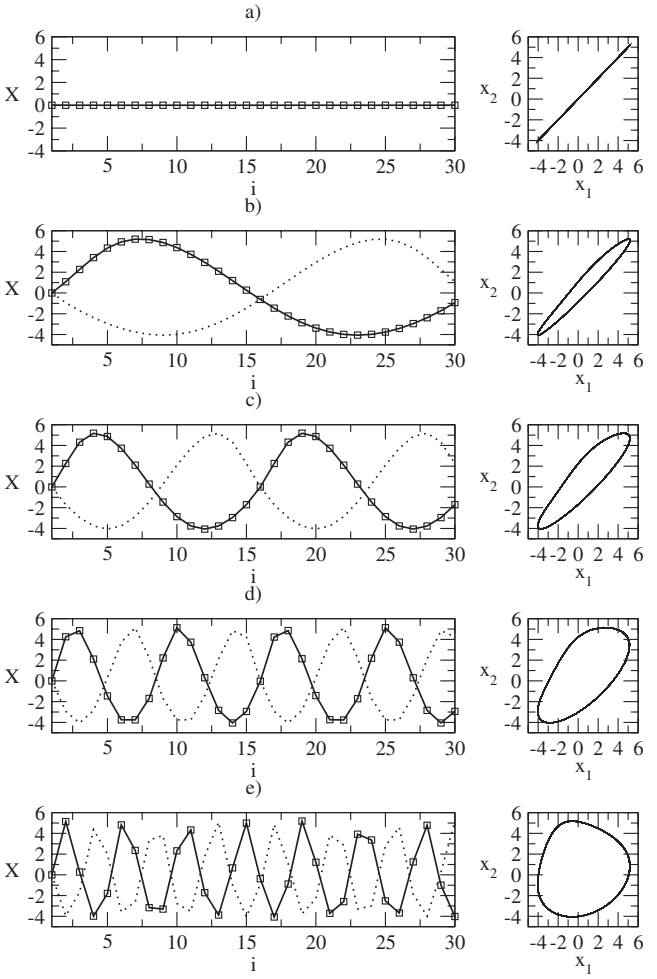


FIG. 2. Snapshots of rotating waves with different index $k\geq 0$ (left-hand panel) and projections of their phase portraits (right-hand panel): (a) $k=0$; (b) $k=1$; (c) $k=2$; (d) $k=4$; and (e) $k=7$. Dotted lines on the left-hand panel depict the snapshots of the backward waves. The values of the parameters are $c=2.35$ and $\gamma=0.005$.

angle, the system converges to the spatially homogeneous wave $1C^0$. Subsequent increasing in $\Delta\phi$ leads to a set of jumps to shorter and shorter waves $1C^0\rightarrow 1C^1\rightarrow\ldots\rightarrow 1C^7$. At $\Delta\phi<\pi/2$, the dependence of the resulting regime on the initial values is regular. Nearby points of $\Delta\phi$ mostly correspond to the same resulting wave. Near and beyond $\Delta\phi=\pi/2$, the dependence is essentially changed. Since none of

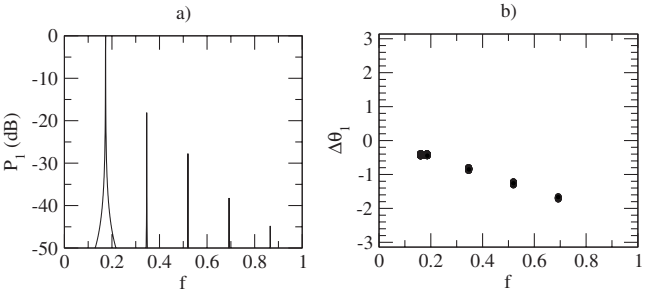


FIG. 3. (a) Power spectrum and (b) phase cross spectrum of $x_1$ oscillations in neighboring sites. The parameters values are the same as in Fig. 2.

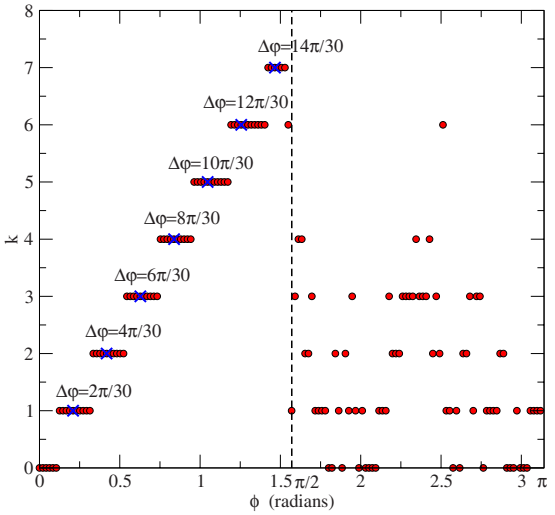


FIG. 4. (Color online) Dependence of type of RW appearing at cyclic choice of initial values (19) on angle $\Delta\phi$. The values of $\Delta\varphi^{(k)}$ are denoted by crosses. The values of parameters are $c=2.7$ and $\gamma=0.005$.

the RW has the value of its phase shift in this range, we observe a random dependence of the resulting regime on the initial conditions. Even nearby initial values may lead to different regimes in the long term limit.

Our special choice of the initial values (19) does not answer the question how typical the different RWs are and it does not allow to evaluate their basins of attraction. For this purpose, we used randomly distributed initial values

$$x_i = X_0 \xi_i^{(x)},$$

$$y_i = Y_0 \xi_i^{(y)},$$

$$z_i = Z_0 \xi_i^{(x)}, \tag{20}$$

where $\xi_i^{(x,y,z)}$ are uncorrelated random numbers uniformly distributed within the interval $[-1;1]$, $X_0=1$, $Y_0=0.5$, $Z_0=1$ are constants. The results of the simulation are summarized in Fig. 5, which plots the probabilities $p^{(k)}$ of the appearance of a certain $k$ mode versus $k$ for two different values of parameter $c$: $c=1.35$ and $c=2.7$. The investigation demonstrates that the two longest modes with $k=0$ and $k=1$ are typical solutions for systems (18). Together they appear with a probability of about 85%. The remaining 15% of initial conditions converge to shorter waves with $k=2$, 3, and 4. The regimes with $k \geq 5$ were not observed with up to 2000 different random initial values. For both parameter values, the dependence is qualitatively similar. However, with increasing $c$ the appearance of shorter waves becomes more probable.

Thus, the investigation of random initial values gives us the possibility to conclude that rotating wave regimes are typical modes for the dynamics in the diffusively coupled chain of oscillators. With random initial values, they appear with almost 100% probability. No other than RW regimes have been observed in the system. The values of the probabilities of different waves allow to evaluate their relative

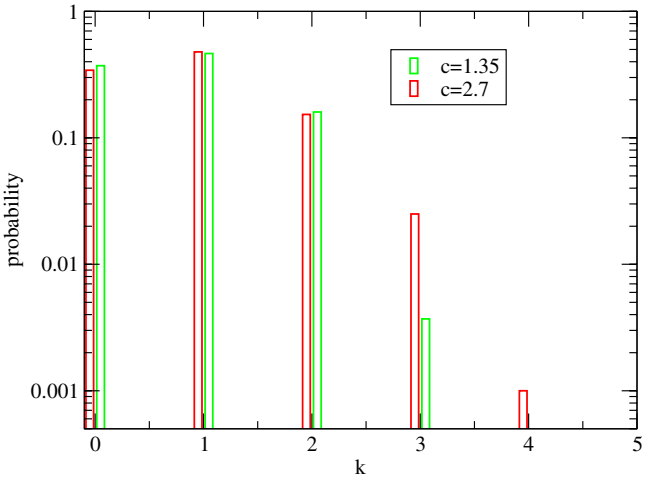


FIG. 5. (Color online) Probabilities $p^{(k)}$ of different RW at $c=1.35$, $\gamma=0.005$ and $c=2.7$, $\gamma=0.005$.

basins of attraction. They must correlate with the values of $p^{(k)}$. We can conclude that the two longest waves $1C^0$ and $1C^1$ have the largest basins, while the basins of the other ones are negligibly small in comparison to them and decrease in size with increasing index $k$.

## IV. EVOLUTION OF RW REGIMES WITH CHANGE IN THE CONTROL PARAMETER

With increasing $c$, the uncoupled Rössler oscillator demonstrates a cascade of period-doubling bifurcations, starting with $1C \rightarrow 2C$ at $c=2.85$ until the transition to chaos at $c \simeq 4.35$. In the chaotic region, band-merging bifurcations and periodic windows are observed. This evolution leads to the one-band chaotic attractor of spiral type, which with further increase in $c$ is changed to the developed funnel chaotic attractor. The behavior of the coupled system generally resembles this scenario; however, it has its peculiarities.

Let us consider the evolution of spatiotemporal behavior of systems (18) with a gradual increase in $c$ at weak coupling $\gamma=0.005$. We choose initial values related to one of the RW then increase slowly $c$ and look for bifurcations taking place on the base of the chosen wave. Repeating this scenario for RW with different $k$, we find the following general properties:

(1) The evolution of the spatially homogeneous oscillations with $k=0$ takes place through the cascade of period-doubling bifurcations, repeating the evolution of the uncoupled oscillator.

(2) Behavior of other RW with $k \neq 0$ differs from spatially homogeneous oscillations. They demonstrate a cascade of period-doubling bifurcations with the replacement of the first bifurcation by the sequence (i) birth of a two-dimensional torus and (ii) saddle-node bifurcation on the torus. The last ones are accompanied by a symmetry breaking when one self-symmetric quasiperiodic solution generates several period-two cycles which are symmetric to each other.

(3) RW with high-period limit-cycles and many-band chaotic attractors can have "defects" in their spatial structure,

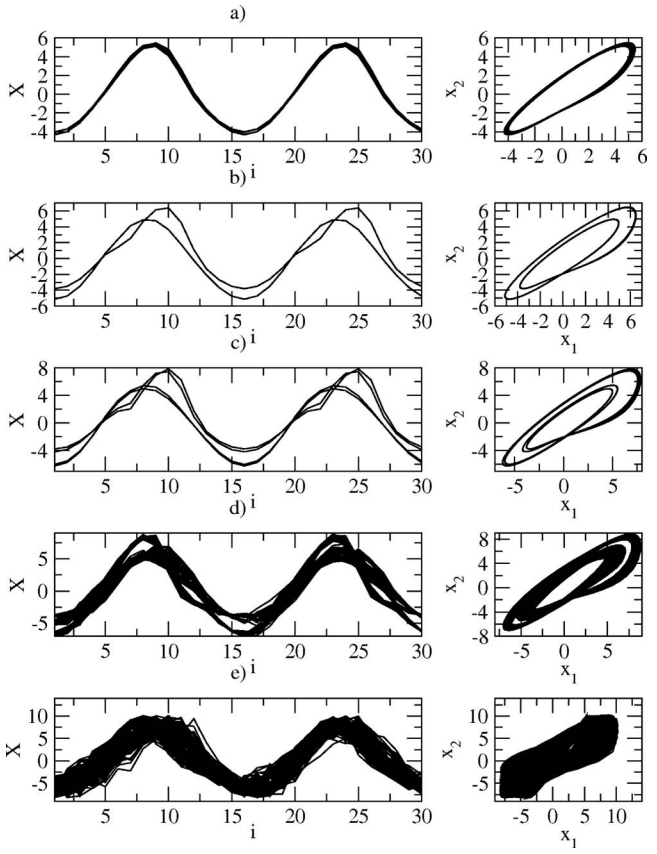


FIG. 6. Snapshots and phase portraits of oscillations originating from $1C^2$ with increasing $c$: (a) $c=2.85$, (b) $c=3.05$, (c) $c=4.1$, (d) $c=4.4$, and (e) $c=6.25$.

when several oscillators in the chain oscillate with the distinct phases of the subharmonics compared to their neighbors. The presence of these defects increases the number of coexisting attractors.

(4) The oscillation with complex temporal behavior inherits the spatial structure from the initial period-one RW. The phase differences at the main frequency are equal to each other in every oscillator of the chain: $\Delta\theta_i^{(1)}=2\pi k/N$. The sum of the phase shifts $\Phi$ keeps its initial value during the evolution from the period-one limit cycle to the one-band chaotic attractor.

Let us consider the evolution of the regimes in more detail. In Fig. 6 we depict several successively complicated oscillations appearing from the wave $1C^2$ [see Fig. 2(c)] with increasing $c$. All of them are characterized by the same spatial structure as the original wave. Two maxima and two minima appear along the chain, which exist on the whole route to chaos [Figs. 6(a)–6(c)] and even inside the chaotic region [Figs. 6(d) and 6(e)]. At $c\simeq 2.8$, the uncoupled oscillator undergoes a period-doubling bifurcation. By contrast, in the array of oscillators we observe a transition from periodic to quasiperiodic behavior [Fig. 6(a)], which is followed by the transition to a period-two limit cycle at $c\simeq 3.05$ [Fig. 6(b)]. This change in the bifurcation mechanism, namely, that the period-doubling bifurcation is replaced by the sequence of torus-birth and saddle-node bifurcation on the torus, is typical for systems of two coupled identical oscillators [5,7,20,21]. In [15], this peculiarity was also shown for an array of Chua' generators.

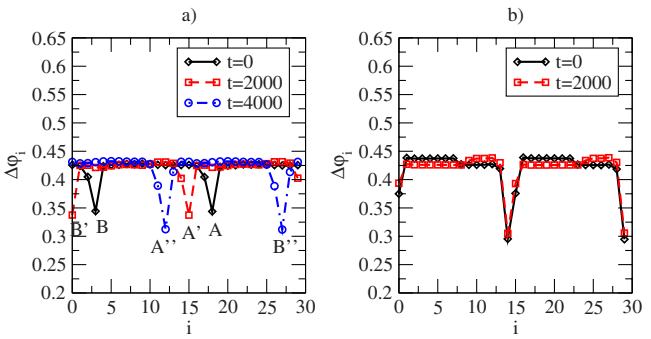


FIG. 7. (Color online) (a) Moving ($c=2.9$, $\gamma=0.01$) and (b) frozen ($c=3.05$, $\gamma=0.01$) phase defects.

The quasiperiodic oscillations appearing after the bifurcation have their special feature. The whole chain exhibits period-two oscillations with phase shifts equal to each other, except for several distinct sites whose phase shifts take other values. The location of these defect oscillations moves along the ring with constant velocity. In the distribution of phase shifts along the chain, we observe several moving "phase defects." The number of defects appears to be equal to the value of index $k$. Hence, the considered mode with $k=2$ in the regime of quasiperiodic oscillations exhibits two such defects. Figure 7(a) depicts the distribution of phase shifts along the chain in three successive instants of time $t=0,2000,4000$ for the wave described in Fig. 6(b). Here, we see two phase defects (marked as "$A$" and "$B$"), which simultaneously move along the array with constant speed. The three successive locations of the defects are marked by $A,A',A''$ and $B,B',B''$, respectively. Thus, we have oscillations with two different time scales: the period of oscillations in every oscillator and the rotation period of the defects round the ring. With increasing $c$, the speed of the rotation is getting slower and, at $c\simeq 3.05$, it becomes equal to zero. The defects "freeze" [Fig. 7(b)] and the oscillations become periodic.

After the transition to period-two oscillations, the new $2C^2$ attractors [Fig. 6(b)] are characterized by the same values of the phase of the main harmonic $\Delta\theta_i^{(1)}$ in every site as its predecessor $1C^2$. However, the distribution of phase shifts along the chain has two frozen phase defects. The spectral analysis of the oscillations has shown that their presence is connected with the phases of the new subharmonic $\Delta\theta_i^{(1/2)}=\Delta\theta_i(0.5f_0)$, appearing after the doubling of the period. Figure 8 depicts the phase portraits (top panels) and phase cross spectra (bottom panels) of oscillations in the "regular" part of the chain [Fig. 8(a)] and inside one of the defects [Fig. 8(b)]. It is seen that while the phases at the main frequency take equal values in both cases, the phases of the subharmonic ($\Delta\theta_i^{(1/2)}$) have more "degrees of freedom." In the considered oscillators, they can take two different values: $0.5\Delta\theta^{(1)}$ in regular oscillators [Fig. 8(a)] and $0.5\Delta\theta^{(1)}+\pi$ in defect oscillators [Fig. 8(b)]. Let us divide the whole array into pairs of neighboring oscillators: $X_1=\{x_1,x_2\}$, $X_2=\{x_2,x_3\}$, … $X_{N-1}=\{x_{N-1},x_N\}$, $X_N=\{x_N,x_1\}$. Every pair can be

in one of the two possible states: "regular" if $\Delta\theta_i^{(1/2)} = 0.5\Delta\theta_i(f_0)$ or defect if $\Delta\theta_i^{(1/2)} = \pi + 0.5\Delta\theta_i(f_0)$. We denote the first state by letter "$a$" and the second one by letter "$b$." So the particularly chosen period-two regime can be denoted by the sequence of letters: $aaa\ldots ba\ldots$. For example, the regime described in Fig. 9(b) with two defects "frozen" in the locations $i=1$ and $i=15$ can be written as the sequence $\underbrace{a\ldots a}_{13}bb\underbrace{a\ldots a}_{13}bb$. However, the regime shown in Fig. 6(b) is not the only oscillation of $k=2$ mode. Evidently, due to the translation symmetry of systems (18), there are 14 additional attractors, which are symmetric to each other and which can be obtained by shifting the variables by $1,2,\ldots,14$ steps. The symmetric regime obtained by shifting by one step has the notation $b\underbrace{a\ldots a}_{13}bb\underbrace{a\ldots a}_{13}b$, the next one $bb\underbrace{a\ldots a}_{13}bb\underbrace{a\ldots a}_{13}$, and so on until the shift by 15 steps when the new regime coincides with the initial one. Thus, after the transition from period-one to period-two oscillations the initial $1C^2$ mode "splits" to 15 submodes, each of which is attributed to the location of the phase defects inside the array. The evolution of each of these submodes takes place the same way.

Further complication of the shape of oscillations takes place via a cascade of period-doubling bifurcations, which leads to many-band chaotic attractors $2C^2 \to 4C^2 \to 8C^2 \ldots \to$chaos. After the transition to chaos, there are band-merging bifurcations of many-band chaotic attractors [there is a two-band attractor in Fig. 6(d)], which lead to a one-band chaotic attractor [Fig. 6(e)].

The evolution of the temporal behavior through the sequence of bifurcations from a simple $1C^2$ wave to spiral chaos keeps the spatial structure of the oscillations, the sum of phase shifts $\Phi$, and the value of the phase at the main frequency in every oscillator $\Delta\theta_i^{(1)}$. Figure 9 depicts cross phase spectra for some typical regular and chaotic regimes of the $k=2$ family: period-four cycle [Fig. 9(a)], two-band [Fig. 9(b)], and one-band [Fig. 9(c)] chaotic attractors. It is seen that in the last cases, the phase of the main harmonic is locked in the same value as the phase of the original period-one cycle.

## V. DEVELOPMENT OF MULTISTABILITY WITH COMPLICATION OF OSCILLATIONS

In the previous section, we have demonstrated that the gradual complication of the shape of oscillations does not violate its spatial structure and the phase relations attributed to the wave. So, high-period periodic, quasiperiodic, and even chaotic oscillations which appeared on the basis of a period-one rotating wave can be considered as RW with more complex temporal behavior. Therefore, in the phase space of systems (18), there are 15 different spatial modes with $k=0,\pm1,\ldots,\pm7$. How many of these modes can be found simultaneously at the chosen parameters values? In Fig. 10 we show the location of each mode in the parameter plane. This figure demonstrates qualitative similarity with that for harmonic oscillations shown in Fig. 1. Every line $L_i$ bounds the region of stability of the corresponding mode with $k=i$. The regions themselves are distinguished by different gray scales: darker colors correspond to shorter waves.

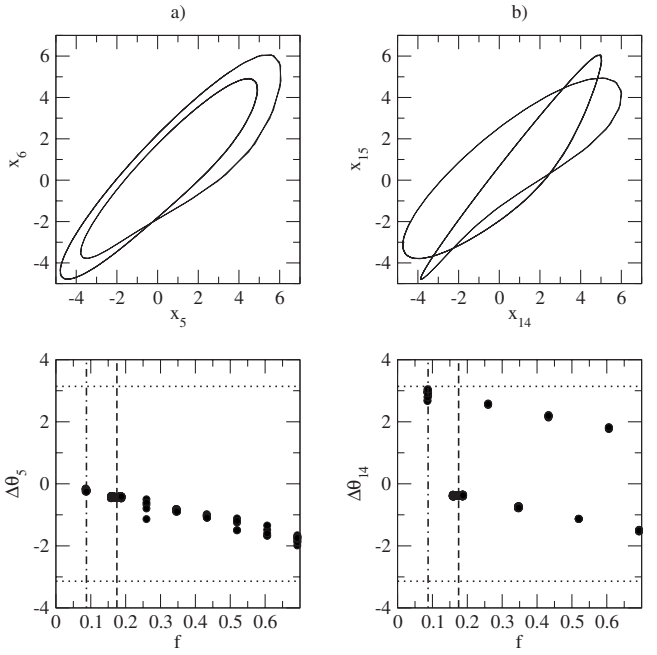


FIG. 8. Phase portrait (top) and phase cross spectrum of oscillations in (a) regular and (b) defect elements. The vertical lines mark frequency of the main harmonic $f=f_0$ (dashed line) and of the first subharmonic $f=f_0/2$ (dot-dashed line). The values of parameters are $c=3.05$, $\gamma=0.01$.

We see a similar structure of encapsulated domains as in Fig. 1. The regions of shorter waves are located inside the regions of longer ones. Hence, at small coupling we can expect at least 15 different attractors in phase space. How does the number of coexisting attractors change with increasing complexity of the oscillations?

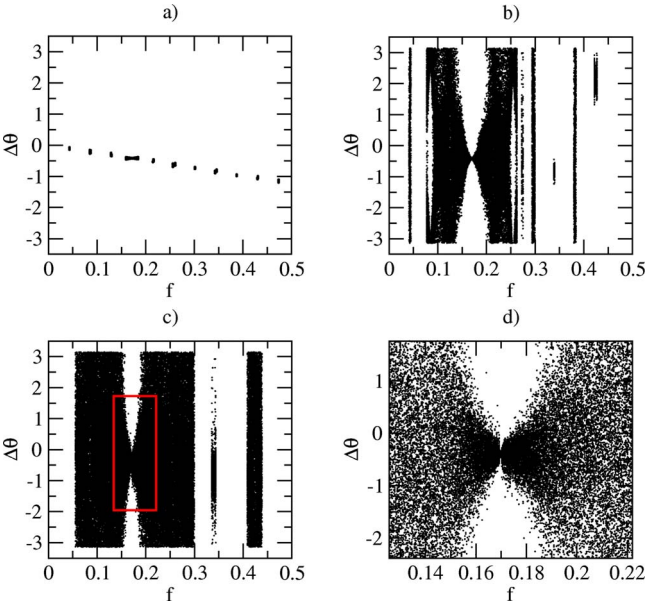


FIG. 9. (Color online) Phase cross spectrum of oscillations of $k=2$ family of regimes: (a) period-four limit cycle [Fig. 6(c)], (b) two-band chaotic attractor [Fig. 6(d)], (c) one-band chaotic attractor [Fig. 6(e)], and (d) the part of figure (c) inside the rectangle.

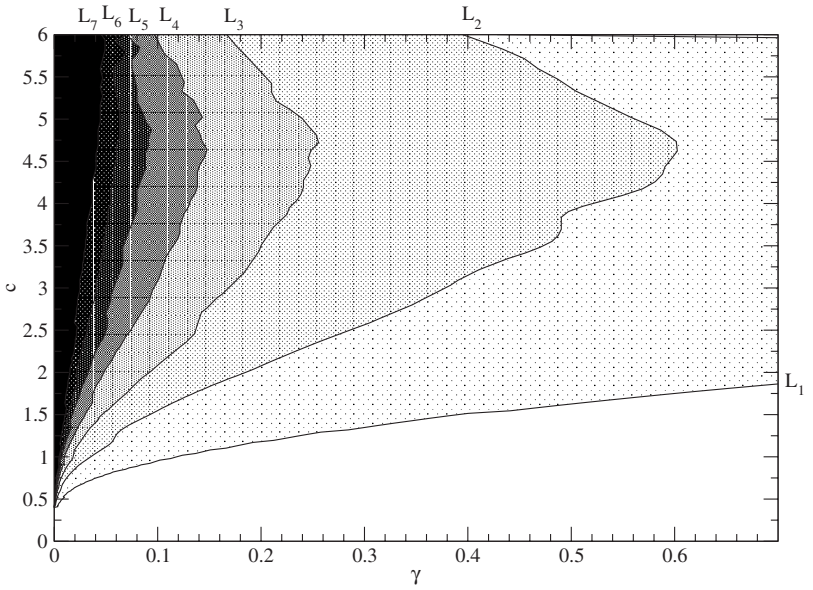


FIG. 10. Location of family of regimes with different $k$ on parameters space $\gamma-c$. The regions occupied by regimes with different $k$ are marked by different grayscales from white for $k=0$ to black for $k=7$. The darker color relates to the shorter wave. Lines $L_i$ mark boundaries of waves with $k=i$.

After the transition from period-one to period-two oscillations, a symmetry breaking of the attractors occurs: one self-symmetric $1C^k$ wave gives birth to several $2C^k$ waves which are symmetric to each other. For example, for the $k=2$ mode, this leads to 15 attractors. Every one of these 15 attractors is characterized by its location of the phase defects. As we have found, the number of defects of period-two oscillations coincides with the index $k$ and the defects are distributed homogeneously along the array. So we can expect that after the transition to period-two oscillations, the number of coexisting attractors must increase as $\sim NM_1$, where $M_1$ is the number of coexisting period-one waves. However, our investigations have revealed that this value is in fact much larger. To evaluate the number of coexisting attractors, we carried out a numerical simulation of systems (18) starting from random initial values (20). In Fig. 11(a), we plot the dependence of the number of attractors found using $I$ sets of initial values. We see that this number grows almost linearly with $I$ and has no tendency to saturate. It manifests that this value significantly exceeds 1931 attractors found after 2000 different runs; hence, this number is much larger than $\sim 450$ expected attractors. For comparison in Fig. 11(b), we computed the same dependency for period-one oscillations. Here we observe saturation after approximately 800 sets of initial values in nine coexisting attractors related to small values of $k=0, \pm 1, \pm 2, \pm 3, \pm 4$.

To evaluate the number of period-two attractors and their types, we consider different waves with $k=2$ at randomly chosen initial values. Figure 12 depicts two examples of such regimes, which we got from two different random initial values. Both presented waves have the same spatial structure with two maxima and two minima along the chain. They are also characterized by the same value of the phases of their main harmonics in the cross spectrum $\Delta\theta_i^{(1)}=-0.418$. The differences between these regimes appear to be defined by the values of the phases of the subharmonics. Their distribution along the chain is depicted on the right side of the figure. Here we observe that the chain contains oscillations in neighboring sites of two types: with the phase of the subharmonics $\Delta\theta_i^{(1/2)}=0.5\Delta\theta_i^{(1)}=-0.209$ (element $a$) and $\Delta\theta_i^{(1/2)}=0.5\Delta\theta_i^{(1)}+\pi=2.932$ (element $b$). Note that the considered waves have another structure than the example described in the previous section [Fig. 6(b)]. They have more than two defects and the defects are located nonuniformly along the chain. Hence, they appear to be a result of other bifurcations than described there. The analysis of Fig. 12 and of the corresponding pictures of other period-two regimes allows us to formulate the hypothesis that the number of both elements $a$ and $b$ and their location can be arbitrary in the chain. In this case, an arbitrary $2C^2$ regime can have any combination of $a$ and $b$ oscillations and, hence, the whole number of corresponding period-two regimes $M_2$ of the particular mode is $2^{N-1}$ [since only $N-1$ pairs are independent, but the $N$th pair is determined by the first and $(N-1)$th pair],

$$M_2 = M_1 2^{N-1}. \tag{21}$$

In the case of $N=30$ elements, it gives the value of 80 530 636 890 coexisting regimes, which evidently exceeds the possibility of numerical checking.

The huge number of period-two attractors does not allow us to check the hypothesis on the considered system of 30 oscillators. However, it can be checked for shorter lattices.

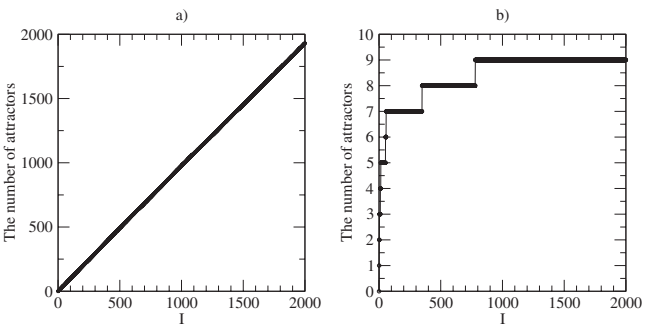


FIG. 11. The number of coexisting attractors found with $I$ sets of randomly chosen initial values for (a) period-two ($c=3.15$) and (b) period-one ($c=2.7$) oscillations.

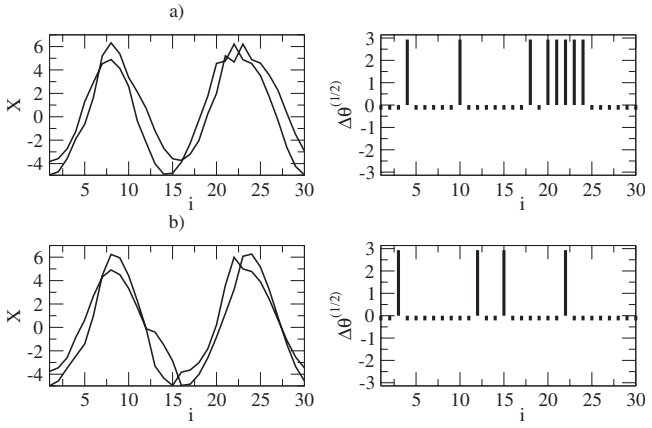


FIG. 12. Two attractors of $2C^2$ mode at $c=3.15$ and $\gamma=0.005$ found at two random initial values. The right-hand figures depict values of phases of the first subharmonic in cross spectra depending on the location of the oscillator.

For $N=2,3,5,6$, the expression (21) predicts $M_2=2,4,48,96$ attractors, respectively. $N=4$ is a special case since it includes $\pi/2$ waves, which are neutrally stable at harmonic approximation. The investigation shows that some of the $\pi/2$ waves with period-two behavior exist at very small coupling $\gamma \leq 0.005$. Nevertheless, for simplicity we exclude the case of $N=4$ from our consideration. The numerical simulations support the expected number of attractors for the short arrays. In Fig. 13 the number of found period-two attractors is plotted versus the number of chosen initial values for $N=3$ and $N=5$. In the both cases, we observe fast saturation of the plot to the predicted values: 4 and 48 attractors, respectively. Similar results are obtained for $N=2$ and $N=6$ arrays.

The further evolution of oscillations based on each of the $M_2$ attractors takes place via period doublings. After every period doubling, we observe the same behavior of phases of the new sub-sub-…-sub-harmonics as in the case of period-two oscillations. For example, after transition to period-four oscillations the phase of the first sub-sub-harmonic $\Delta\theta_i^{(1/4)}=\Delta\theta_i(0.25f_0)$ can take two different values $\Delta\theta_i^{(1/2)}/2$ or $\pi+\Delta\theta_i^{(1/2)}/2$, where $\Delta\theta_i^{(1/2)}$ is the phase of the first subharmonic in the chosen pair of oscillators. Hence, each of the $M_2$ period-two attractors gives birth to $2^{N-1}$ period-four attractors, and the whole number of period-four attractors is expected to be

$$M_4 = M_1 4^{N-1}.$$

It predicts 16 attractors in an array of three oscillators and 768 attractors in an array of five oscillators. The results of the numerical simulations are presented in Fig. 13 as well. In the first case, the expected value after which the number of found attractor remains constant is reached sufficiently quickly [Fig. 13(a)]. In the second case, the value has not been reached after 10 000 different runs, but we observe convergence of extrapolation of the plot to it [see Fig. 13(b)]. Extrapolating the rule for period-two and period-four attractors for other high-periodic ones, we obtain the number of coexisting period-$i$ limit cycles,

$$M_i = M_1 i^{N-1}. \tag{22}$$

Formula (22) generalizes the known rule for multistability formation in two coupled period-doubling oscillators [5], where the number of coexisting attractors doubles after every doubling of the period. It gives an infinite number of coexisting attractors at the threshold to chaos and, practically, an infinite number of high-period periodic attractors for sufficiently large chains.

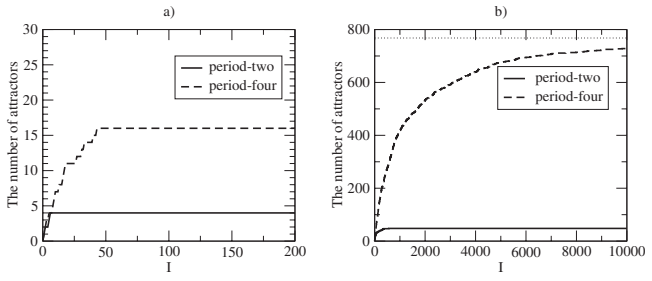


FIG. 13. The number of coexisting period-two ($c=3.15$, $\gamma=0.005$) and period-four ($c=4.1$, $\gamma=0.005$) attractors found after $I$ sets of random initial values for chains (a) of $N=3$ and (b) of $N=5$ oscillators. The dot line in (b) marks the predicted number of 768 attractors.

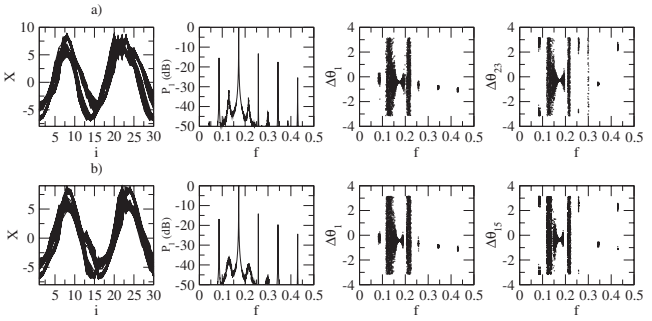


FIG. 14. Two-band chaotic attractors formed on the base of period-two cycles depicted in Fig. 12; $c=4.4\gamma=0.005$.

After the transition to chaos on the base of every period-$i$ cycle, an $i$-band chaotic attractor is formed. Band-merging bifurcations of chaotic attractors are accompanied by merging of the attractors originated from different limit cycles. As a result, the number of coexisting chaotic attractors successively decreases after every bifurcation. This can be explained in terms of their power and phase spectra. The transition from a $2^n$-band to a $2^{n-1}$-band attractor means a "dissolving" of the $n$th subharmonic in the power spectrum of oscillations and of the corresponding unlocking of their phases. This can be demonstrated using the example of the transition between two-band and one-band chaotic attractors whose phase portraits, power spectra, and phase cross spectra are depicted in Figs. 14(a), 14(b), 9(c), and 9(d). In Figs. 14(a) and 14(b), we built snapshots, power spectrum, and two phase cross spectrum of chaotic waves originating from the period-two cycles depicted in Figs. 12(a) and 12(b). The phase cross spectra are calculated for two different sites in the array, where the original limit-cycles exhibited oscillations of $a$ type and $b$ type. We see that the values of the

phases of subharmonics of the predecessors are inherited by the chaotic attractors. Phases on "dissolved" sub-subharmonics are uniformly distributed on the $[-\pi;\pi]$ interval. Hence, CRW inherits the phase defects of the periodic RW on the base of which they have been formed and the number of two-band attractors must be equal to the number of period-two cycles. Therefore, for the evaluation of the number of chaotic attractors, we have the same formula as that for periodic cycles. After the sequence of band-merging bifurcations in phase space, there are 15 chaotic RW characterized by the same value of $\Phi=2\pi k$, $k=0,\pm 1,\ldots,\pm 7$ as the original period-one cycles. Their spatial structures [see Fig. 6(e)] are inherited from the structures of periodic rotating waves.

## VI. PHASE SYNCHRONIZATION BETWEEN OSCILLATORS IN THE REGIME OF CHAOTIC RW

Spatial order demonstrated in the regime of chaotic RW must evidently be a consequence of synchronization between oscillators in the chain, which typically takes the form of chaotic phase synchronization (PS). PS is the phenomenon of instantaneous phase locking [22], which is also characterized by frequency adjustment [23] and coherence increase [24]. Phase synchronization can be formally defined as the boundedness of the difference between instantaneous phases $\psi_{A,B}$ of the time series from subsystems $A$ and $B$,

$$\lim_{t\to\infty}|\psi_A(t)-\psi_B(t)|<R, \tag{23}$$

where $R$ is a positive value. This relation indicates the presence of correlations between phases, while instantaneous amplitudes remain uncorrelated. Besides the full phase synchronization defined by Eq. (23), there is an "imperfect" PS [25]. This means that instantaneous phases remain locked during sufficiently long but finite time intervals, after which the phase difference "slips" to the next locked value. As a result, on the average the phase difference goes slowly to infinity.

The main problem in investigating chaotic phase synchronization is the correct definition of phases for oscillations of complex shape. The instantaneous phases are known to be well defined when the chaotic attractor is quite "good," namely, when its spectrum has a well-distinguished peak on a frequency corresponding to some preferable time scale of oscillations. Therefore, oscillators with coherent chaos are typical models to investigate the phenomenon of chaotic phase synchronization. We restrict ourselves to the spiral-type chaos where different definitions for the instantaneous phase give quantitatively similar results [26]. In our approach, we define the instantaneous phase $\psi_i(t)$ of chaotic oscillations just "unwrapping" the phases [Eq. (2)] from the interval $[-\pi;\pi]$ to the semi-interval $[-\pi;\infty[$,

$$\psi_i(t)=\varphi_i(t)+2\pi n,$$

where $n$ is the number of jumps of the function $\varphi_i(t)$ to the value $-2\pi$. Besides instantaneous phases, we will look at the coherence function $\sigma_{ij}$ of $x_i(t)$ and $x_j(t)$ oscillations,

$$\sigma_{ij}(f)=\left|\frac{C_{ij}(f)}{\sqrt{P_i(f)P_j(f)}}\right|,$$

where $C_{ij}(f)=\langle F_i(f)F_j^*(f)\rangle$ is the power cross spectrum. The function $\sigma_{ij}(f)$ characterizes qualitatively the locking of the Fourier phases on the chosen frequency $f$: $\sigma_{ij}(f)=1$ at the frequencies where differences between the Fourier phases remain constant ($\theta_i(f)-\theta_j(f)=$const) and $\sigma_{ij}(f)\to 0$ at those frequencies where the phases are totally independent and, hence, their differences $\theta_i(f)-\theta_j(f)$ take random values uniformly distributed in $[-\pi;\pi]$ [the strict equality $\sigma_{ij}(f)=0$ holds if the number of data points approaches infinity].

To observe the phenomenon of PS more clearly, we introduce a small mismatch between neighboring oscillators,

$$\begin{aligned}\dot{x}_i&=\Delta_i(-y_i-z_i)+\gamma(x_{i+1}-2x_i+x_{i-1}),\\ \dot{y}_i&=\Delta_i(x_i+0.2y_i),\\ \dot{z}_i&=0.2+z_i(x_i-c),\end{aligned} \tag{24}$$

where $\Delta_i$ is the parameter of the mismatch. $\Delta_i$ is equal to 1 for odd $i$ and to $1+\Delta(\Delta\ll 1)$ for even $i$. The value of $\Delta_i$ influences the basic frequency of uncoupled oscillations, so our modification allows us to study an array of slightly detuned oscillators, when each oscillator surrounded by two neighbors with frequencies differing from its own by equal values.

Let us consider systems (24) at $c=6.5$, which is related to the one-band spiral chaos in the uncoupled oscillator and at $\gamma=0.025$. At these values of the parameters, both in the symmetrical ($\Delta=0$) and in the slightly mismatched ($\Delta=0.001$) systems there are 15 chaotic RW with $k=0,\pm 1,\ldots,\pm 7$ coexisting in phase space. The portraits of several of them, namely, those which originated from the waves in Fig. 2 are depicted in Fig. 15. Every CRW is characterized by a constant value of $k(t)=k$, as well as the full coherence of the oscillations on the main frequency and its harmonics, while the coherence on other frequencies is essentially less than 1 [see Fig. 16(a)]. Will these properties preserve at smaller coupling? We choose the initial values which correspond to the shortest wave with $k=7$. Then we gradually decrease the coupling toward zero and look for the change in the behavior of $k(t)$. For this purpose, we built the "bifurcation diagram" in terms of $k$. We compute the values $k(t)$ during the interval $t_0<t<t_0+T$ ($t_0=30\,000$ is the time of relaxation, $T=2000$ is the interval of observation) for each value of $\gamma$. The results of this study are presented in Fig. 17. We see that the whole interval of coupling can be quantitatively divided into two subintervals: $\gamma\geq 0.002$ with constant $k$ and $0\leq\gamma<0.002$ (marked by gray color) with drifting $k$. In the first interval, we observe subsequent "jumps" from shorter waves to longer ones until $k=1$. So, the mode with $k=7$ changes to the mode with $k=6$ at $\gamma\simeq 0.018$, then to $k=5$ at $\gamma\simeq 0.0065$, $k=4$ at $\gamma\simeq 0.0042$, and so on.

Every mode with constant $k(t)$ represents the typical case of phase synchronization of chaos with locking of instantaneous phases near some determined value. To support this conclusion, we plot the difference between instantaneous phases $\Delta\psi_{1,2}(t)$ in time in Fig. 18(a) for $k=7$ and $k=2$. The

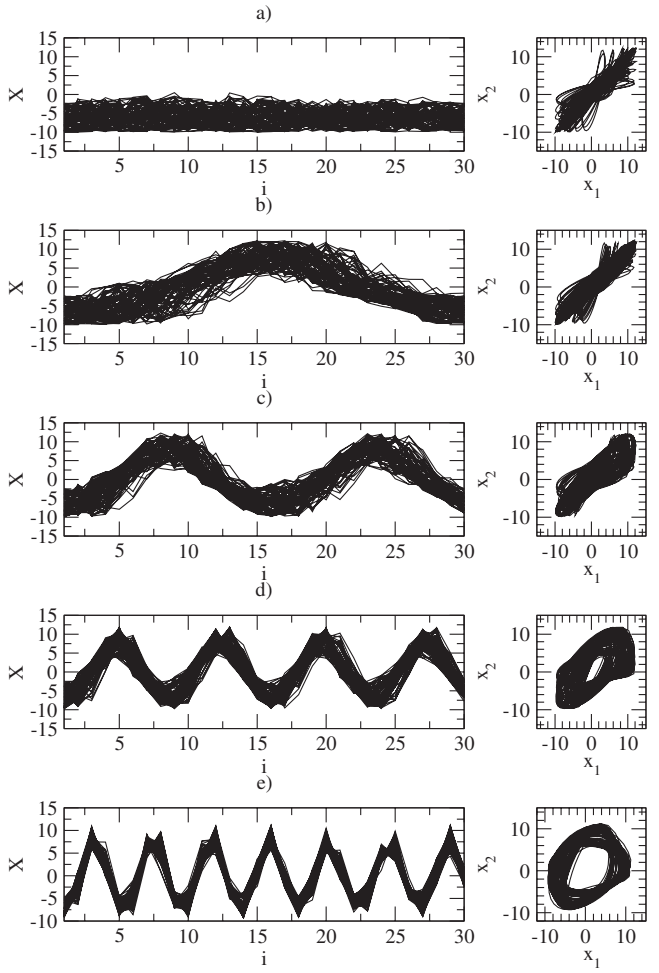


FIG. 15. Snapshots of chaotic RW (left hand) and projections of the phase portraits (right hand) with (a) $k=0$, (b) $k=1$, (c) $k=2$, (d) $k=4$, and (e) $k=7$; $c=6.25$, $\gamma=0.025$.

instantaneous phases are locked near the values of the phases of main harmonics $\Delta\theta^{(1)}$. The power spectra and the coherence functions are similar to those in Fig. 16(a).

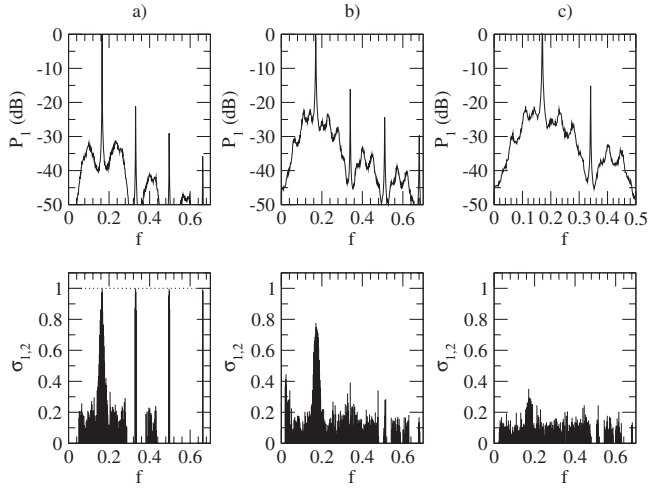


FIG. 16. (Top) Power spectrum and (bottom) coherence function of one-band chaotic RW at $c=6.25$ with decreasing coupling: (a) $\gamma=0.025$, (b) $\gamma=0.0012$, and (d) $\gamma=0.0007$.

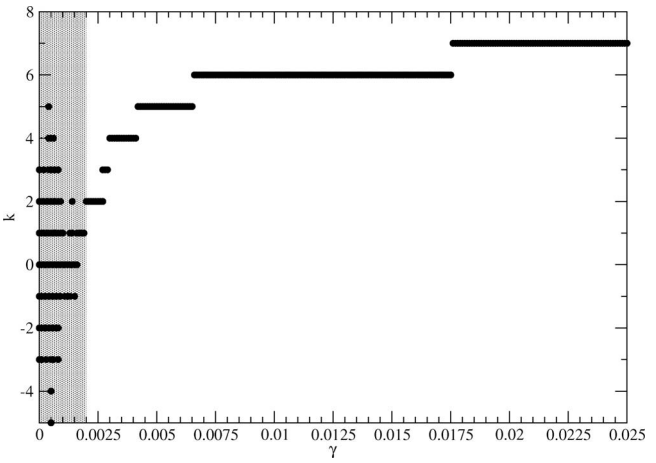


FIG. 17. Dependence of $k(t)$ on coupling strength at $c=6.25$. The region of drifting $k$ is distinguished by the gray color.

After decreasing the coupling strength to $\gamma \leq 0.002$, the behavior is changed. The value $k(t)$ is not constant in time anymore but moves randomly between several integer values. This indicates the break of the spatial order attributed to the chaotic rotating wave and the loss of perfect synchronization. The instantaneous phase difference begins to "diffuse" from one locking state to another as it is shown in Fig. 18(b) (top panel). This can also be seen from the coherence function [Fig. 16(b)], which is less than 1 at the main frequency. The Fourier phases are not locked anymore. The behavior of the coherence function can serve as one more diagnosis tool of the transition from full phase synchronization to the imperfect one [24]. So we can conclude that the behavior of both the instantaneous phases and the coherence function exhibit evidence for the loss of synchronization. Nevertheless, in spite of the case of two coupled oscillators, here the value of the difference between instantaneous phases remains finite in time. Actually, the character of the dynamics looks like an intermittency process between several phase synchronous states. This can be seen in Fig. 18(b) (bottom plane), where we show the time evolution of $k$. It is seen that it does not keep the constant value anymore but

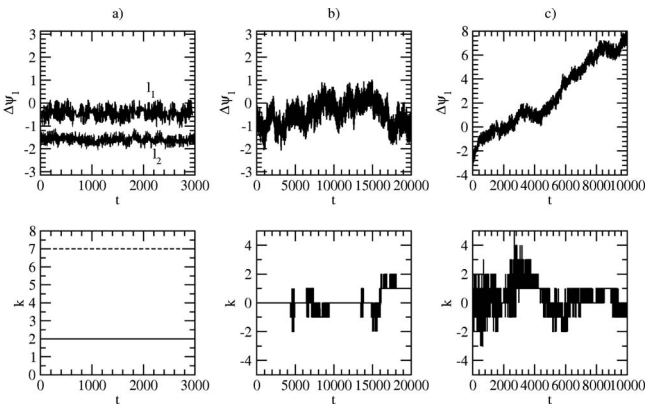


FIG. 18. Time dependence of difference between instantaneous phases $\Delta\psi_1$ (top) and $k$ (bottom) at $c=6.25$ with decreasing coupling: (a) $\gamma=0.025$, (b) $\gamma=0.0012$, and (c) $\gamma=0.0007$. In (a) curve $l_1$ relates to the $k=2$ wave; $l_2$ relates to the $k=7$ wave.

jumps randomly between several values. Between the moments of the jumps, there exist sufficiently long intervals of constant values $k=0$ and $k=\pm 1$.

With further decreasing coupling, at $\gamma \leq 0.001$ we observe another qualitative transition in synchronous behavior. Here, the regime of intermittency between synchronous states is changed to the "classical" imperfect phase synchronization, where the phase difference drifts slowly to infinity, temporally "braking" near some intermediate values. This state is depicted in Fig. 18(c) (top panel). This behavior of instantaneous phases is reflected in the dynamics of $k(t)$. The intervals during which it remains constant are reduced to zero and $k$ jumps permanently between several values. Further decreasing coupling toward zero leads to further vanishing of imperfect synchronization, which, at zero coupling, turns into fully asynchronous oscillations.

## VII. CONCLUSION

We considered the development of phase multistability in an ensemble of self-sustained period-doubling oscillators with symmetric diffusive coupling. In the case of simple period-one oscillations, PM manifests as a sequence of $N/2$ coexisting rotating waves with different wavelengths. These regimes appear with almost 100% probability when choosing initial values randomly.

The transition to high-period oscillations increases the number of attractors. After every period doubling, we find as many attractors as the number of attractors before the bifurcation times $2^{N-1}$. On the threshold to chaos, the number of attractors tends to infinity. In the chaotic region, the tendency is the opposite. Development of chaos via band-merging bifurcations decreases the number of coexisting attractors by a factor $2^{N-1}$ after every bifurcation. As a result, the number of coexisting period-$i$ limit cycles coincides with the number of coexisting $i$-band chaotic attractors. This process results in $N/2$ chaotic rotating waves in the regime of one-band spiral chaos.

In the regime of CRW, the array demonstrates the phenomenon of chaotic phase synchronization between neighboring oscillators. Gradual decreasing coupling strength leads first to a transition from shorter waves to longer ones. Then, at very small coupling, the regime of chaotic rotating waves turns into intermittency between several waves. This is accompanied by the loss of locking of the phase of the main harmonic in the cross spectrum and, thus, loss of full phase synchronization between the oscillators. The phase synchronization becomes imperfect, though the value of phase difference does not go to infinity, but drifts within a limited interval between several values. At last, after further decreasing coupling toward values close to zero, this type of oscillations is changed to classical imperfect synchronization behavior with intervals of temporal locking of the phases which are connected by phase slips.

Our results generalize the regularities of development of phase multistability observed in two coupled oscillators [5,8] to a network of an arbitrary length. We found out that arrays with several elements, which do not possess multistability themselves, can demonstrate a huge number of coexisting attractors being weakly coupled. The spatial structure, which appears already after the first period-doubling bifurcation, is characterized by the presence of a number of phase defects, whose quantity and location are practically unpredictable. This leads to unpredictable spatial structures which can be observed in sufficiently small networks of simple periodic oscillators. The last property can be important both for understanding of fundamental laws of nature since many phenomena observed in physics, biology, chemistry, and other sciences are results of collective behavior of many interacting oscillator and, from practical point of view, for example, for tasks of coding of information and memory storage, etc.

## ACKNOWLEDGMENTS

A.S. thanks the Ministry of Education and Science of Russian Federation and to the German Academic Exchange Service (DAAD) for the financial support of the research (Program "Mikhail Lomonosov").

[1] R. D. Li and T. Erneux, Phys. Rev. A **49**, 1301 (1994).
[2] S. Nichols and K. Wiesenfeld, Phys. Rev. E **50**, 205 (1994).
[3] A. D. Defontaines, Y. Pomeau, and B. Rostand, Physica D **46**, 201 (1990).
[4] T. Erneux and G. Nicolis, Physica D **67**, 237 (1993).
[5] V. V. Astakhov, B. P. Bezruchko, E. N. Erastova, and E. P. Seleznev, Sov. Tech. Phys. Lett. **35**, 1122 (1990); T. E. Vadivasova, O. S. Sosnovtseva, A. G. Balanov, and V. V. Astakhov, Discrete Dyn. Nat. Soc. **4**, 231 (2000); E. Mosekilde, D. E. Postnov, and O. V. Sosnovtseva, Prog. Theor. Phys. **150**, 147 (2003).
[6] A. G. Balanov, N. B. Janson, V. V. Astakhov, and P. V. E. McClintock, Phys. Rev. E **72**, 026214 (2005).
[7] V. S. Anishchenko, T. E. Vadivasova, V. V. Astakhov, O. V. Sosnovtseva, C. W. Wu, and L. O. Chua, Int. J. Bifurcation Chaos Appl. Sci. Eng. **5**, 1677 (1995); V. V. Astakhov, A. V. Shabunin, A. N. Silchenko, G. I. Strelkova, and V. S. Anishchenko, J. Commun. Technol. Electron. **42**, 294 (1997); V. V. Astakhov, A. V. Shabunin, and V. S. Anishchenko, *ibid.* **42**, 907 (1997); B. P. Bezruchko, M. D. Prokhorov, and E. P. Seleznev, Chaos, Solitons Fractals **15**, 695 (2003).
[8] V. Astakhov, A. Shabunin, T. Kapitaniak, and V. Anishchenko, Phys. Rev. Lett. **79**, 1014 (1997); V. Astakhov, M. Hasler, T. Kapitaniak, A. Shabunin, and V. Anishchenko, Phys. Rev. E **58**, 5620 (1998); V. Astakhov, A. Shabunin, W. Uhm, and S. Kim, *ibid.* **63**, 056212 (2001).
[9] P. Ashwin, G. P. King, and J. W. Swift, Nonlinearity **3**, 585 (1990); D. G. Aronson, M. Golubitsky, and J. Mallet-Paret, *ibid.* **4**, 903 (1991).
[10] L. Angelini, G. Lattanzi, R. Maestri, D. Marinazzo, G. Nardulli, L. Nitti, M. Pellicoro, G. D. Pinna, and S. Stramaglia, Phys. Rev. E **69**, 061923 (2004).

[11] G. B. Ermentrout, J. Math. Biol. **23**, 55 (1985); SIAM J. Appl. Math. **52**, 1665 (1992); L. Ren and G. B. Ermentrout, Physica D **143**, 56 (2000).
[12] V. I. Nekorkin and V. A. Makarov, Phys. Rev. Lett. **74**, 4819 (1995).
[13] H. Daido, Phys. Rev. Lett. **78**, 1683 (1997).
[14] M. A. Matias, V. Perez-Munuzuri, I. P. Marino, M. N. Lorenzo, and V. Perez-Villa, Europhys. Lett. **37**, 379 (1997); M. A. Matias, V. Perez-Munuzuri, M. N. Lorenzo, I. P. Marino, and V. Perez-Villar, Phys. Rev. Lett. **78**, 219 (1997); I. P. Marino, V. Perez-Munuzuri, V. Perez-Villar, E. Sanchez, and M. A. Matias, Physica D **128**, 224 (1999).
[15] A. Shabunin, V. Astakhov, and V. Anishchenko, Int. J. Bifurcation Chaos Appl. Sci. Eng. **12**, 1895 (2002).
[16] V. I. Nekorkin, V. A. Makarov, and M. G. Velarde, Int. J. Bifurcation Chaos Appl. Sci. Eng. **6**, 1845 (1996).
[17] A. S. Gurtovnik and Y. I. Neimark, *Proceedings of Dynamics of System* (N. Novgorod State University, , 1991), p. 84.
[18] O. E. Rössler, Phys. Lett. A **57**, 397 (1976).
[19] S. L. Marple, *Digital Spectral Analysis with Applications* (Prentice-Hall, Englewood Cliffs, NJ, 1987).
[20] T. Hogg and B. A. Huberman, Phys. Rev. A **29**, 275 (1984).
[21] J. Rasmussen, E. Mosekilde, and C. Reick, Math. Comput. Simul. **40**, 247 (1996).
[22] M. G. Rosenblum, A. S. Pikovsky, and J. Kurths, Phys. Rev. Lett. **76**, 1804 (1996).
[23] V. S. Anishchenko, T. E. Vadivasova, D. E. Postnov, and M. A. Safonova, Int. J. Bifurcation Chaos Appl. Sci. Eng. **2**, 633 (1992).
[24] A. Shabunin, V. Astakhov, and J. Kurths, Phys. Rev. E **72**, 016218 (2005).
[25] M. A. Zaks, E.-H. Park, M. G. Rosenblum, and J. Kurths, Phys. Rev. Lett. **82**, 4228 (1999).
[26] V. S. Anishchenko, T. E. Vadivasova, and G. I. Strelkova, Fluct. Noise Lett. **4**, L219 (2004).